

# Rotational and Quasiviscous Cold Flow Models for Axisymmetric Hybrid Propellant Chambers

**Joseph Majdalani**

H. H. Arnold Chair of Excellence in Advanced Propulsion and Professor  
e-mail: majj@utsti.edu

**Michel Akiki**

Mechanical, Aerospace and Biomedical Engineering Department,  
University of Tennessee Space Institute,  
Tullahoma, TN 37388

*In this work, we present two simple mean flow solutions that mimic the bulk gas motion inside a full-length, cylindrical hybrid rocket engine. Two distinct methods are used. The first is based on steady, axisymmetric, rotational, and incompressible flow conditions. It leads to an Eulerian solution that observes the normal sidewall mass injection condition while assuming a sinusoidal injection profile at the head end wall. The second approach constitutes a slight improvement over the first in its inclusion of viscous effects. At the outset, a first order viscous approximation is constructed using regular perturbations in the reciprocal of the wall injection Reynolds number. The asymptotic approximation is derived from a general similarity reduced Navier–Stokes equation for a viscous tube with regressing porous walls. It is then compared and shown to agree remarkably well with two existing solutions. The resulting formulations enable us to model the streamtubes observed in conventional hybrid engines in which the parallel motion of gaseous oxidizer is coupled with the cross-streamwise (i.e., sidewall) addition of solid fuel. Furthermore, estimates for pressure, velocity, and vorticity distributions in the simulated engine are provided in closed form. Our idealized hybrid engine is modeled as a porous circular-port chamber with head end injection. The mathematical treatment is based on a standard similarity approach that is tailored to permit sinusoidal injection at the head end. [DOI: 10.1115/1.4002397]*

## 1 Introduction

The substitution of hybrid propellants in propulsive applications is gradually gaining popularity as demonstrated in the effective use of a nitrous oxide/HTPB combination for the main engine of the 2004 SpaceShipOne suborbital vehicle. Having been initiated in the early seventies, research devoted to enhancing hybrid engine performance continues to receive attention today in both academic and commercial sectors. In this vein, one may cite Chiaverini, Knuth, Karabeyoglu, Kuo, Krier, and others [1–7] whose notable achievements have been reflected in the design and testing of innovative chamber and propellant configurations. However, most of these studies have been experimentally focused and the mathematical models used to obtain hybrid regression rate correlations have often assumed one-dimensional gaseous motion above the grain surface. The need for more elaborate analytical formulations, such as those required to approximate the velocity field above the propellant boundary, has been recently identified in a survey by Kuo and Chiaverini [8] as one of the impediments confronting the development of future hybrid models. Thus given an idealized representation of a cylindrical hybrid chamber with axial symmetry, it is the purpose of this study to investigate the suitability of two approximations of increasing order of accuracy that may be used to describe the attendant two-dimensional flow field.

In a typical hybrid, an inert solid fuel grain burns in the presence of a gaseous or liquid oxidizer (see Fig. 1). The resulting diffusion flame resembles that of a household candle: While the hot reacting gases compel the fuel to pyrolyze and vaporize, the oxidizer and fuel particles combust along the exposed port areas in several layers of decreasing fuel concentration. This process is illustrated in Fig. 2 where stacked layers of decreasing fuel fractions are shown to separate the oxidizer from the solid fuel grain.

In 1966, a simple analytical solution was proposed by Culick [9] for describing the mean gaseous motion in a solid rocket motor (SRM). His solution was derived under the contingencies of steady, incompressible, rotational, axisymmetric, and inviscid (high Reynolds number) flow. It coincided with Taylor's 1956 solution obtained in a different physical context [10,11]. The resulting profile was scrutinized in subsequent studies, including computational [12–14], experimental [14–17], and theoretical investigations [18–23]; it was found to be quite adequate for modeling the mean flow in a full-length cylindrical motor. To this date, Culick's profile remains at the foundation of several theoretical studies, especially, those concerned with acoustic instability [24–26]. Despite its simplicity and dismissal of SRM physicochemistry, it has proven to be quintessential in investigating several performance-related mechanisms that are germane to rocket motor internal ballistics [17,19,20,27].

In a simplified model of a hybrid propellant chamber, the motion of gases ejected along the grain can be assumed to be normal to the surface, as in the case of SRMs. In fact, a closed-form analytical approximation, namely, one that will be pursued here, can be used to describe the gas motion corresponding to this idealized representation of a hybrid chamber. If slip is allowed at the surface, another solution can be managed, albeit irrotational. In either of the two cases, the interactions within the flame zone must be ignored lest an intractable problem is reached at leading order. Instead, the burning surface will be modeled, as in the case of a solid propellant, by assuming a porous surface [9]. The difference here lies in the mass injection across the wall, which will be (an order of magnitude) smaller than in the case of a solid propellant. The technique that we consider relies on a conventional similarity approach. This will be employed in conjunction with Euler's equations whose application is justified in view of the (still) appreciable injection Reynolds numbers that accompany this problem. The goal will be to reconstruct a steady, slightly viscous, incompressible mean flow solution for a full-length circular-port hybrid engine. Naturally, the solutions suggested in the past for SRMs with similar conditions will have to be modified to include the incoming flow of oxidizer from the head end. This has been

Contributed by the Fluids Engineering Division of ASME for publication in the JOURNAL OF FLUIDS ENGINEERING. Manuscript received May 2, 2009; final manuscript received August 16, 2010; published online October 12, 2010. Assoc. Editor: Joseph Katz.

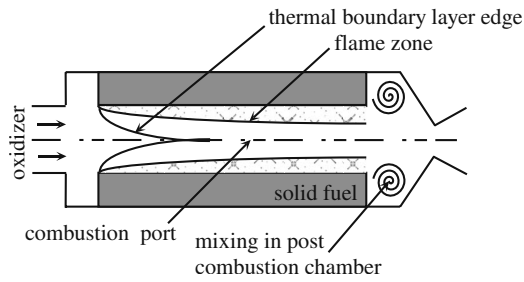


Fig. 1 Schematic of the circular-port hybrid rocket

partly accomplished by Majdalani and Saad [28] in a recent study of the Taylor–Culick profile with arbitrary headwall injection. However, their analysis was strictly focused on the construction of inviscid series approximations and computational verifications of the flow field with arbitrary headwall injection. Until more refined models become available, the idealization that we seek may be viewed as a first-cut, far field approximation due to the three main reasons that will be expounded next.

Unlike SRMs, the burning rate of hybrid rocket fuel is very sensitive to the flow field in the chamber [29,30]. Hence, many standard assumptions, such as uniform burning, which can be justified in SRMs, become less suitable in hybrids.

The validity of the inviscid solution for SRMs has been shown to be adequate at high injection Reynolds numbers, generally, exceeding 500 [14–17]; this is easily satisfied in SRMs where large burning rates produce Reynolds numbers in excess of 1000. In hybrid chambers, the fuel burning rate remains an order of magnitude smaller [31], albeit sufficiently large to justify an asymptotic treatment in which viscosity can be properly incorporated. The construction of a viscous solution appears to be more essential here than in the case of SRMs, especially that viscous effects will have a more pronounced impact on pressure than velocity. With this feature in mind, a viscous rotational approximation will be provided as a more accurate alternative.

The real challenge of hybrid propulsion stands in the mixing and burning of the two streams. However, in seeking a basic description, no attempts will be made to consider the mixing of the oxidizer and fuel or to model the burning of the two streams. These desirable pursuits will be deferred to later studies in which nonuniform burning, mixing, and the effect of particle-mean flow interactions may be separately addressed.

## 2 Hybrid Model

The basic hybrid engine can be modeled as a cylindrical chamber of porous length  $L$  and radius  $a$  with both a permeable head end and a fully open downstream end. The permeable head end permits the injection of a fluid at a prescribed velocity profile. A sketch of the chamber is given in Fig. 3 where  $\bar{r}$  and  $\bar{z}$  are used to denote the radial and axial coordinates. The field of interest extends from the head end to the nozzle's attachment point at the

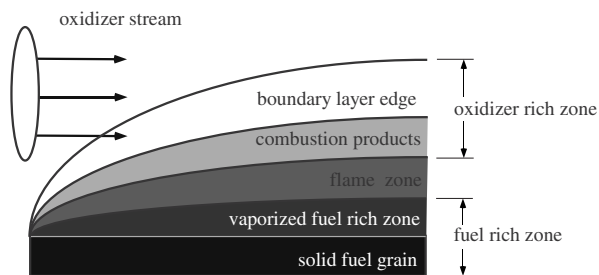


Fig. 2 Decreasing fuel concentration zones above solid surface during hybrid grain pyrolysis

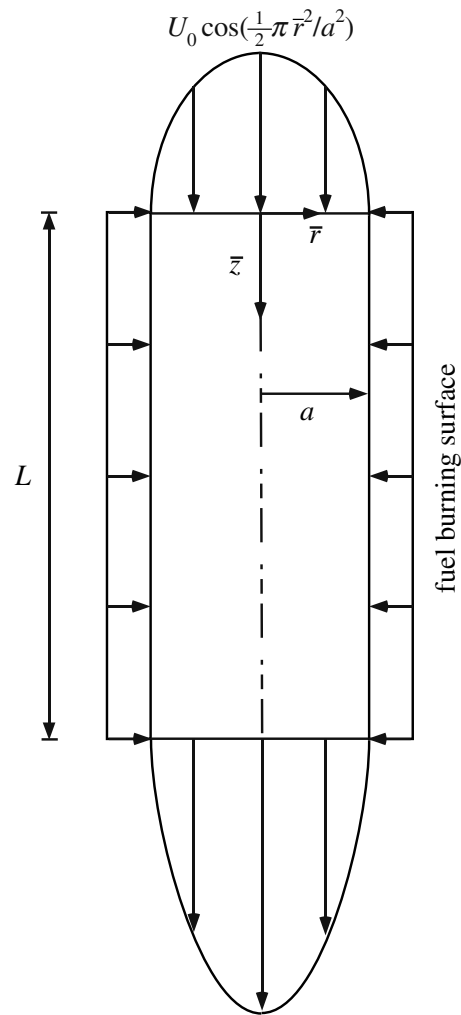


Fig. 3 Sketch of the rotational full-length hybrid model depicting mass addition along both sidewall and endwall boundaries. Here the oxidizer injection at the head end corresponds to a sinusoidal profile.

base of the chamber. Downstream of the base, the flow is accelerated after expanding through a nozzle whose treatment is not required here. This mathematical model does not take into account the three-dimensional complexity of the nozzle attachment, which will be highly variable depending on specific design shapes and nozzle types. In this vein, compressibility effects are discounted with the flow being controlled by conditions established upstream of the nozzle location. Using the present study as a starting point, a more elaborate model can be later constructed that would include nozzle effects, interactions with the flame sheet, etc.

At the head end, an oxidizer stream is injected into the chamber at a maximum centerline speed equal to  $U_0$ . This incoming oxidizer merges with the peripheral flux caused by uniform mass addition at the porous sidewall. The sidewall injection velocity  $U_w$  is used to represent the solid fuel regression rate. Clearly,  $U_w$  can be appreciably smaller than  $U_0$  due to typical rates of fuel pyrolysis. This condition can be later exploited in seeking an asymptotic approximation of higher order. The current analysis seeks to capture the essential features of the ensuing flow field using a sinusoidal head end injection profile, namely,

$$\bar{u}_z(\bar{r}, 0) = U_0 \cos\left(\frac{1}{2} \pi \bar{r}^2 / a^2\right) \quad (1)$$

The corresponding motion arises naturally due to the developing rotational flow field in a porous tube with normal sidewall mass addition [10,32].

**2.1 Equations.** A nonreactive flow can be considered, prompted by the low volumetric heat release that accompanies diffusion flames. Furthermore, the basic flow can be assumed to be (i) steady, (ii) incompressible, (iii) rotational, and (iv) axisymmetric. Based on these assumptions, the Navier–Stokes equations become

$$\frac{1}{\bar{r}} \frac{\partial(\bar{r}\bar{u}_r)}{\partial\bar{r}} + \frac{\partial\bar{u}_z}{\partial\bar{z}} = 0 \quad (2)$$

$$\bar{u}_r \frac{\partial\bar{u}_r}{\partial\bar{r}} + \bar{u}_z \frac{\partial\bar{u}_r}{\partial\bar{z}} = -\frac{1}{\rho} \frac{\partial\bar{p}}{\partial\bar{r}} + \nu \left[ \frac{\partial^2\bar{u}_r}{\partial\bar{z}^2} + \frac{\partial}{\partial\bar{r}} \left( \frac{1}{\bar{r}} \frac{\partial(\bar{r}\bar{u}_r)}{\partial\bar{r}} \right) \right] \quad (3)$$

$$\bar{u}_r \frac{\partial\bar{u}_z}{\partial\bar{r}} + \bar{u}_z \frac{\partial\bar{u}_z}{\partial\bar{z}} = -\frac{1}{\rho} \frac{\partial\bar{p}}{\partial\bar{z}} + \nu \left[ \frac{\partial^2\bar{u}_z}{\partial\bar{z}^2} + \frac{1}{\bar{r}} \frac{\partial}{\partial\bar{r}} \left( \bar{r} \frac{\partial\bar{u}_z}{\partial\bar{r}} \right) \right] \quad (4)$$

Note that the effect of the wall regression on the mean flow is neglected in most analyses of SRMs [19,20]. It can be safely ignored in the case of hybrids due to their relatively slower regression.

**2.2 Boundary Conditions.** The boundary conditions are due to symmetry, no slip at the sidewall, and both head end and sidewall injection. Specifically, one can assume

- uniform injection along the cylindrical sidewall,
- vanishing axial flow in fulfillment of the no slip boundary condition at the sidewall,
- a prescribed injection pattern at the head end and
- vanishing radial velocity along the centerline.

These particulars can be written as

$$\begin{cases} \bar{r} = a, & 0 \leq \bar{z} < L, & \bar{u}_r = -U_w & \text{(sidewall injection)} \\ \bar{r} = a, & 0 \leq \bar{z} < L, & \bar{u}_z = 0 & \text{(no slip at the wall)} \\ \bar{z} = 0, & \forall \bar{r}, & \bar{u}_z = U_0 \cos\left(\frac{1}{2}\pi\bar{r}^2/a^2\right) & \text{(endwall)} \\ \bar{r} = 0, & \forall \bar{z}, & \bar{u}_r = 0 & \text{(no flow across centerline)} \end{cases} \quad (5)$$

**2.3 Normalization.** In seeking a similarity solution, it is helpful to normalize all variables and operators. This can follow

$$z = \frac{\bar{z}}{a}, \quad r = \frac{\bar{r}}{a}, \quad \nabla = a\nabla, \quad p = \frac{\bar{p}}{\rho U_w^2} \quad (6)$$

$$u_r = \frac{\bar{u}_r}{U_w}; \quad u_z = \frac{\bar{u}_z}{U_w}; \quad u_0 = \frac{U_0}{U_w} \quad (7)$$

Here  $U_0 = \bar{u}_z(0,0)$  and  $U_w = -\bar{u}_r(a,\bar{z})$  represent the maximum fluid injection velocity at the head end and the uniform wall injection velocity at the sidewall, respectively. The corresponding boundary conditions reduce to

$$\begin{cases} u_r(1,z) = -1 \\ u_z(1,z) = 0 \\ u_z(r,0) = u_0 \cos\left(\frac{1}{2}\pi r^2\right) \\ u_r(0,z) = 0 \end{cases} \quad (8)$$

At this point, the vorticity transport equation,  $\nabla \times \mathbf{u} \times \boldsymbol{\Omega} = \mathbf{0}$ , may be solved in conjunction with the constraints granted by Eq. (8).

**2.4 Rotational Solution.** For a sinusoidal head end injection velocity, the vorticity stream function approach can be applied by introducing

$$u_r = -\frac{1}{r} \frac{\partial\psi}{\partial z}, \quad u_z = \frac{1}{r} \frac{\partial\psi}{\partial r} \quad (9)$$

Substitution into  $\nabla \times \mathbf{u} \times \boldsymbol{\Omega} = \mathbf{0}$  yields

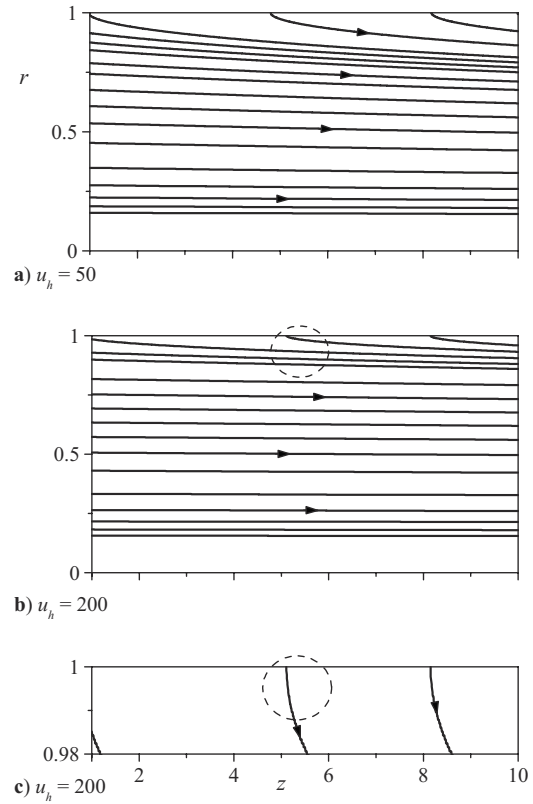


**Fig. 4 Rotational streamlines shown for two increasing head end injection parameters. The inset in part (c) corresponds to a magnified section of part (b) illustrating the normal sidewall injection feature.**

$$\frac{\partial\psi}{\partial z} \frac{\partial}{\partial r} \left( \frac{\Omega_\theta}{r} \right) = \frac{\partial\psi}{\partial r} \frac{\partial}{\partial z} \left( \frac{\Omega_\theta}{r} \right), \quad \Omega_\theta = \frac{\partial u_r}{\partial z} - \frac{\partial u_z}{\partial r} \quad (10)$$

This expression will be satisfied when  $\Omega_\theta/r = F(\psi)$ . In seeking a closed-form solution, we insert  $\Omega_\theta = C^2 r \psi$  into the vorticity equation and collect

$$\frac{\partial^2\psi}{\partial z^2} + \frac{\partial^2\psi}{\partial r^2} - \frac{1}{r} \frac{\partial\psi}{\partial r} + C^2 r^2 \psi = 0 \quad (11)$$

Similarly, the boundary conditions may be written for the stream function. Based on Eq. (8), we have

$$\begin{cases} \frac{1}{r} \frac{\partial\psi(1,z)}{\partial z} = -1, & \frac{1}{r} \frac{\partial\psi(1,z)}{\partial r} = 0 \\ \frac{1}{r} \frac{\partial\psi(r,0)}{\partial r} = u_0 \cos\left(\frac{1}{2}\pi r^2\right), & \frac{1}{r} \frac{\partial\psi(0,z)}{\partial z} = 0 \end{cases} \quad (12)$$

Then using separation of variables, we let  $\psi(r,z) = f(r)g(z)$  and reduce Eq. (11) into

$$-\frac{g''}{g} = \frac{f''}{f} - \frac{1}{r} \frac{f'}{f} + C^2 r^2 = \pm \lambda^2 \quad (13)$$

One may infer from Eq. (12) that the derivative of  $g(z)$  must be a constant to ensure a linear variation in  $z$ . The case of  $\lambda=0$  is selected, thus leading to  $f = A \cos\left(\frac{1}{2}Cr^2\right) + B \sin\left(\frac{1}{2}Cr^2\right)$  and  $g = C_1 z + C_2$ . Subsequent application of Eq. (12) produces, systematically,  $A=0$ ,  $B=C_1^{-1}$ ,  $C=\pi$ , and  $C_2=C_1 u_0/\pi$ . At length, we recover

$$\psi = (z + u_h) \sin\left(\frac{1}{2}\pi r^2\right), \quad u_h \equiv u_0/\pi \quad (14)$$

As shown in Fig. 4, increasing the headwall injection parameter increases the flow turning severity near the sidewall. Specifically,

as  $u_h$  is increased from 50 to 200, the streamlines, which otherwise resemble those of a solid rocket motor, become dominated by axial (parallel-flow) motion everywhere except in the neighborhood of the sidewall. This can be clearly attributed to the increased propensity of the axial stream flowing into the chamber. At larger  $u_h$  the normally injected stream is met by an overwhelmingly larger axial flow that forces it to rapidly turn and assimilate with it. In practice, the values of  $U_0$  and  $U_w$  can be calibrated to reproduce the patterns associated with a prototypical hybrid engine.

Based on Eq. (14), other pertinent variables may be evaluated. For example, one finds

$$u_r = -\frac{1}{r} \sin\left(\frac{1}{2} \pi r^2\right), \quad u_z = \pi(z + u_h) \cos\left(\frac{1}{2} \pi r^2\right),$$

$$\Omega_\theta = \pi^2(z + u_h) r \sin\left(\frac{1}{2} \pi r^2\right) \quad (15)$$

$$\frac{\partial p}{\partial r} = -\frac{-1 + \pi r^2 \sin(\pi r^2) + \cos(\pi r^2)}{2r^3}, \quad \frac{\partial p}{\partial z} = -\pi^2(u_h + z) \quad (16)$$

and, for the pressure drop from the head end, one can put

$$\Delta p = \frac{-1 - 2\pi^2 r^2 z(2u_h + z) + \cos(\pi r^2)}{4r^2} \quad (17)$$

In Fig. 5, the two velocity components, vorticity and the radial pressure drop at the head end, are plotted. While the axial velocity increases linearly with the head end injection parameter, the radial velocity remains unaffected. In fact, the radial component is seen to be identical to its counterpart in SRMs, namely, that of Culick [9]. In Fig. 5(c), the vorticity is seen to be largest near the sidewall where flow is entering perpendicularly to the fuel surface. Away from the wall, vorticity decays rapidly; it approaches zero near the centerline where the flow becomes nearly uniform. As for the pressure drop, Fig. 5(d) illustrates how  $\Delta p(r, 0)$  in the head end plane can surpass its wall value when

$$\frac{1}{2} \sqrt{2} < r < 1 \quad (18)$$

In this range, the largest magnitude corresponds to  $\Delta p = -0.569108$ . This extremum corresponds to  $r_m = 0.861405$  and can be obtained by differentiating Eq. (17) at fixed  $z$ . Note that the radial pressure variation is strongly connected with the radial velocity shown in Fig. 5(b). Both experience an unexpected surge in magnitude immediately after injection, thus exceeding their absolute value at the wall.

### 3 Viscous Rotational Solution

Viscous effects can be accommodated, as performed previously in the context of SRM internal ballistics by Majdalani and co-workers [19,20]. To that end, one can start with the reduced Navier–Stokes equation incorporating both viscosity and wall regression speed. Then by putting  $\alpha = 0$  in Refs. [19,20], we are left with the case corresponding to stationary walls, namely,

$$2\varepsilon \left( \theta \frac{d^4 F}{d\theta^4} + 2 \frac{d^3 F}{d\theta^3} \right) + F \frac{d^3 F}{d\theta^3} - \frac{dF}{d\theta} \frac{d^2 F}{d\theta^2} = 0 \quad (19)$$

where

$$\psi = \frac{\bar{\psi}}{a^2 U_w} = (z + u_h) F, \quad u_r = -\frac{F}{r}, \quad u_z = \frac{(z + u_h) dF}{r dr} \quad (20)$$

The corresponding boundary conditions are

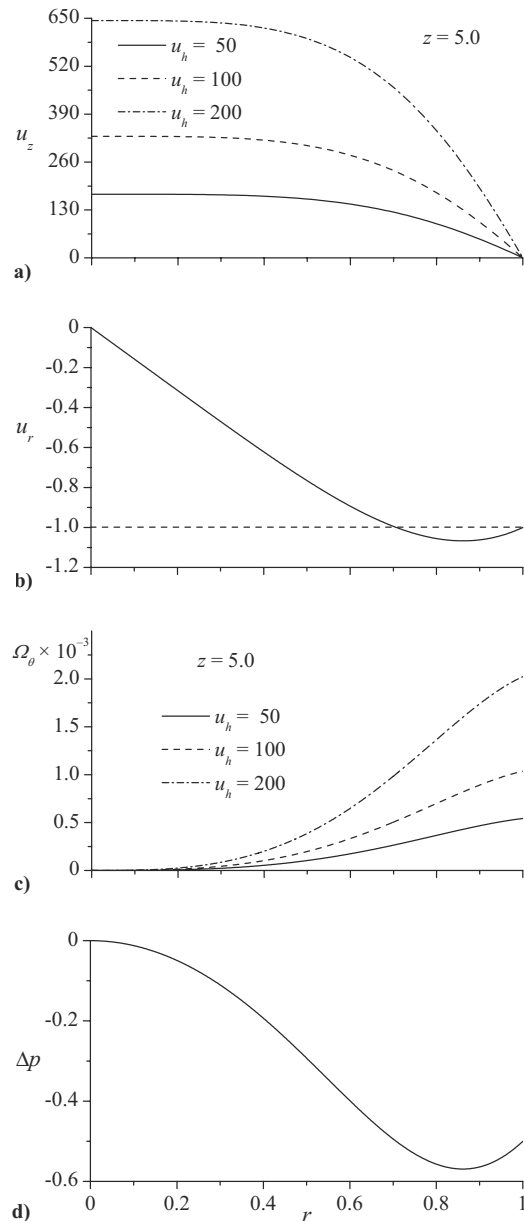


**Fig. 5 Description of (a) axial and (b) radial velocities in addition to (c) vorticity and (d) pressure drop at the chamber's head end. Both axial velocity and vorticity are shown at a fixed axial position.**

$$\frac{dF\left(\frac{1}{2}\pi\right)}{d\theta} = 0, \quad F\left(\frac{1}{2}\pi\right) = 1, \quad F(0) = 0, \quad \lim_{\theta \rightarrow 0} \sqrt{\theta} \frac{d^2 F}{d\theta^2} = 0 \quad (21)$$

Note that  $\varepsilon \equiv \nu / (aU_w)$  is the inverted Reynolds number based on the wall injection velocity.

Equation (19) may be solved asymptotically by first setting  $F = F_0 + \varepsilon F_1 + O(\varepsilon^2)$  and then inserting the expanded form back into Eq. (19). At the leading order, one retrieves

$$F_0 \frac{d^3 F_0}{d\theta^3} - \frac{dF_0}{d\theta} \frac{d^2 F_0}{d\theta^2} = 0 \quad (22)$$

where  $F_0 = \sin \theta$  represents a suitable outcome. The first order equation becomes

$$\frac{d^3 F_1}{d\theta^3} \sin \theta - \frac{d^2 F_1}{d\theta^2} \cos \theta + \frac{dF_1}{d\theta} \sin \theta - F_1 \cos \theta = -2\theta \sin \theta \quad (23)$$

To solve Eq. (23), one can apply the variation of parameters approach twice in succession. To this end, a homogenous solution is introduced in the form of  $F_{1h} = C(\theta) \cos \theta$ , where  $C(\theta)$  is a variable coefficient. Through backward substitution into Eq. (23), one collects

$$C''' \sin \theta \cos \theta - 2C'' \sin^2 \theta - C' = 0 \quad (24)$$

whence

$$C(\theta) = K_0 \tan \theta + K_1 \theta + K_2 \quad (25)$$

With  $C(\theta)$  in hand, the homogenous part becomes

$$F_{1h} = K_0 \sin \theta + K_1 \theta \cos \theta + K_2 \cos \theta \quad (26)$$

At this point, the method of variation of parameters is applied a second time by permitting  $K_0$ ,  $K_1$ , and  $K_2$  to vary in space. Consequently, Eq. (26) is rewritten as

$$F_1(\theta) = K_0(\theta) \sin \theta + K_1(\theta) \theta \cos \theta + K_2(\theta) \cos \theta \quad (27)$$

Then using Eq. (23), one recovers

$$K_0' \sin \theta + K_1' \theta \cos \theta + K_2' \cos \theta = 0 \quad (28)$$

$$K_0' \cos \theta + K_1'(\cos \theta - \theta \sin \theta) - K_2' \sin \theta = 0 \quad (29)$$

and

$$-K_0' \sin^2 \theta - K_1'(2 \sin^2 \theta + \theta \cos \theta \sin \theta) - K_2' \cos \theta \sin \theta = 4 \cos \theta - 2\theta \sin \theta \quad (30)$$

The ensuing set of coupled, first order ordinary differential equations (ODEs) may be solved to obtain

$$K_0 = -2 \csc \theta - \sin \theta - \theta \cos \theta - S(\theta) + C_0 \quad (31)$$

$$K_1 = 2 \csc \theta + S(\theta) + C_1 \quad (32)$$

$$K_2 = -\cos \theta + \theta \sin \theta - 2\theta \csc \theta - S_1(\theta) + C_2 \quad (33)$$

where

$$S(\theta) = \int_0^\theta \phi \csc \phi \, d\phi = \theta + \sum_{k=1}^{\infty} \frac{2}{\pi^{2k}} \left( \sum_{n=1}^{\infty} \frac{1}{n^{2k}} \right) \frac{(1-2^{1-2k})}{(2k+1)} \theta^{2k+1} \quad (34)$$

$$S_1(\theta) = \int_0^\theta \phi^2 \csc \phi \, d\phi = \frac{1}{2} \theta^2 + \sum_{k=1}^{\infty} \left( \sum_{n=1}^{\infty} n^{-2k} \right) \frac{(1-2^{1-2k})}{(k+1)\pi^{2k}} \theta^{2k+2} \quad (35)$$

Thus, by combining the leading and first order solutions, a complete viscous approximation may be expressed as

$$F = \sin \theta + \varepsilon \{ -3 + (\theta \cos \theta - \sin \theta) S(\theta) - S_1(\theta) \cos \theta + C_0 \sin \theta + C_1 \theta \cos \theta + C_2 \cos \theta \} \quad (36)$$

where

$$C_0 = 3 + S\left(\frac{1}{2}\pi\right), \quad C_1 = -6\pi^{-1} - 1 - S\left(\frac{1}{2}\pi\right) + (2/\pi)S_1\left(\frac{1}{2}\pi\right), \quad C_2 = 3 \quad (37)$$

By inspection, it can be seen that, if viscosity is set to zero in Eq. (36), the inviscid form given by Eqs. (14) and (15) will be recovered. In summary, the viscous approximation for the rotational model comprises

$$\psi = (z + u_h) \left[ \sin \theta + \varepsilon \left( -3 + \left[ 3 + S\left(\frac{1}{2}\pi\right) - S(\theta) \right] \sin \theta - \cos \theta \left\{ S_1(\theta) - 3 + \theta \left[ 1 + 6\pi^{-1} + S\left(\frac{1}{2}\pi\right) - S(\theta) - 2\pi^{-1} S_1\left(\frac{1}{2}\pi\right) \right] \right\} \right) \right] + O(\varepsilon^2) \quad (38)$$

$$u_r = -\sqrt{\frac{\pi}{2\theta}} \left[ \sin \theta + \varepsilon \left( -3 + \left[ 3 + S\left(\frac{1}{2}\pi\right) - S(\theta) \right] \sin \theta - \cos \theta \left\{ S_1(\theta) - 3 + \theta \left[ 1 + 6\pi^{-1} + S\left(\frac{1}{2}\pi\right) - S(\theta) - 2\pi^{-1} S_1\left(\frac{1}{2}\pi\right) \right] \right\} \right) \right] + O(\varepsilon^2) \quad (39)$$

$$u_z = \pi(z + u_h) \left[ \cos \theta + \varepsilon \left( -\theta + 2 \left[ 1 - 2\pi^{-1} + \pi^{-1} S_1\left(\frac{1}{2}\pi\right) \right] \cos \theta + \left\{ S_1(\theta) - 3 + \theta \left[ 1 + 6\pi^{-1} + S\left(\frac{1}{2}\pi\right) - S(\theta) - 2\pi^{-1} S_1\left(\frac{1}{2}\pi\right) \right] \right\} \sin \theta \right) \right] + O(\varepsilon^2) \quad (40)$$

As for the corrected pressure drop, it can be obtained by integrating from the centerline to any radius. One gets

$$\begin{aligned} \Delta p_{\perp} &\equiv p(0, z) - p(\theta, z) = \pi \left[ \varepsilon F_{\theta} + \frac{1}{4} \theta^{-1} F^2 - \varepsilon F_{\theta}(0) \right] \\ &= \frac{1}{4} \pi \theta^{-1} \sin^2 \theta + \varepsilon \pi \left( \cos \theta - 1 - \frac{3}{2} \theta^{-1} \sin \theta \right. \\ &\quad \left. + \frac{1}{4} \theta^{-1} \left\{ 3 + S\left(\frac{1}{2}\pi\right) - S(\theta) + \cos(2\theta) \left[ S(\theta) - S\left(\frac{1}{2}\pi\right) - 3 \right] \right\} \right. \\ &\quad \left. + \frac{1}{4} \sin(2\theta) \left\{ S(\theta) - S\left(\frac{1}{2}\pi\right) - 1 - 6\pi^{-1} + 2\pi^{-1} S_1\left(\frac{1}{2}\pi\right) \right\} \right. \\ &\quad \left. + \theta^{-1} \left[ 3 - S_1(\theta) \right] \right) + O(\varepsilon^2) \end{aligned} \quad (41)$$

In like fashion, the pressure drop in the flow direction can be estimated from

$$\begin{aligned} \Delta p_{\parallel} &\equiv p(\theta, 0) - p(\theta, z) \\ &= -\pi^2 z \left( \frac{1}{2} z + u_h \right) \left[ 2\varepsilon (\theta F_{\theta\theta\theta} + F_{\theta\theta}) - (F_{\theta})^2 + F F_{\theta\theta} \right] \\ &= \pi^2 z \left( \frac{1}{2} z + u_h \right) \{ 1 + (2\varepsilon/\pi) [2\pi - 6 + 4\pi C - 7\zeta(3)] \} + O(\varepsilon^2) \end{aligned} \quad (42)$$

where  $C = \frac{1}{2} S\left(\frac{1}{2}\pi\right) \approx 0.91596559$  is Catalan's constant, and  $\zeta(3) \approx 1.2020569$  is the Riemann zeta function defined by  $\zeta(x) = \sum_{k=1}^{\infty} k^{-x}$ . Hence, one can put  $\Delta p_{\parallel} \approx \pi^2 z \left( \frac{1}{2} z + u_h \right) (1 + 2.15123\varepsilon) + O(\varepsilon^2)$ . Finally, the shear stress (or vorticity) can be calculated from

$$\tau = \frac{\bar{\tau}}{\rho U_w^2} = -\varepsilon \Omega = \varepsilon z \sqrt{2} \pi^{3/2} \sqrt{\theta} F_{\theta\theta} = -\varepsilon z \sqrt{2} \pi^{3/2} \sqrt{\theta} \sin \theta + O(\varepsilon^2) \quad (43)$$

At the wall, one is left with  $\tau_w = -\varepsilon z \pi^2 + O(\varepsilon^2)$ .

The viscous solution presented above is the result of a similarity transformation in space and time. Results, obtained using this approach, are illustrated in Fig. 6 at several Reynolds numbers ranging from 5 to  $\infty$  (for inviscid conditions). The three parts in Fig. 6 correspond to the main characteristic function  $F$ , as well as both axial and radial velocities. Note that the influence of viscous damping is most pronounced near the centerline, as reflected in the flow smoothing or laminarization affecting the axial velocity in Fig. 6(b). This may also explain the steeper top-hat profiles associated with the inviscid solution. The characteristic function  $F$  and the radial velocity undergo a similar, albeit less appreciable flattening process.

In Fig. 7, the first order correction function  $F_1$  is compared with two existing solutions developed, first, by Yuan and Finkelstein [33] and, second, by Terrill and Thomas [34]. These are derived in the context of a porous cylinder with stationary walls. For the Yuan-Finkelstein expression, we have

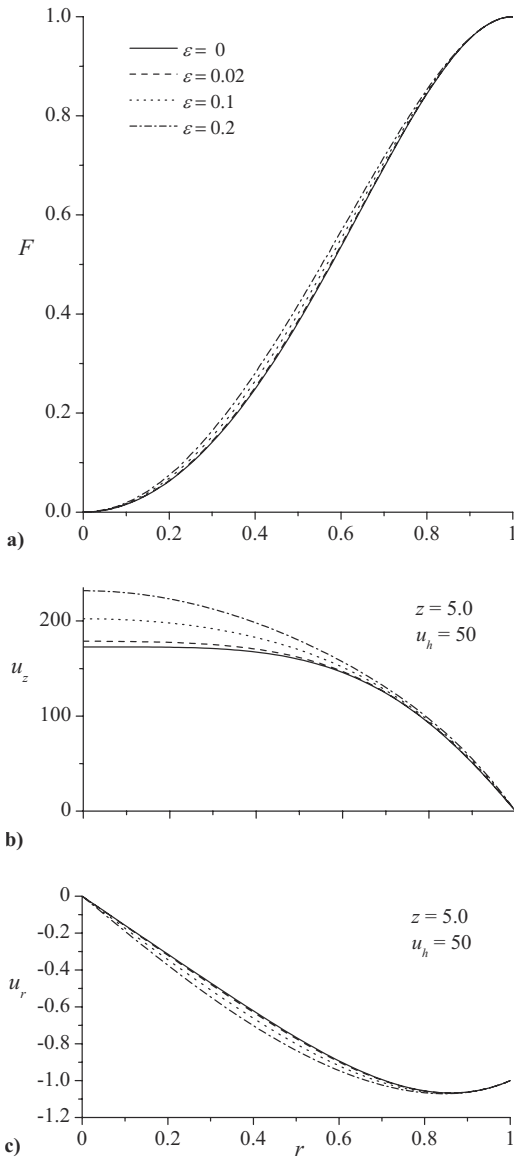


**Fig. 6** Description of (a) the main characteristic function  $F$  along with the corresponding (b) axial and (c) radial velocities. Broken lines depict the flow where  $\varepsilon=0.02, 0.1$  and  $0.2$  whereas solid lines correspond to the inviscid flow field.

$$\begin{aligned}
 F = \sin \theta + \varepsilon \left\{ \left[ 3 - \frac{1}{8} \pi^3 \int_0^1 \xi^2 \csc\left(\frac{1}{2} \pi \xi\right) d\xi \right. \right. \\
 \left. \left. - \frac{1}{8} \pi^3 \int_1^{(2/\pi)\theta} \xi^2 \csc\left(\frac{1}{2} \pi \xi\right) d\xi \right] \cos \theta - (3 + 8 \pi^{-2} k_1 \sin \theta) \right\} \\
 + \left[ 1 + 6 \pi^{-1} - \frac{1}{4} \pi^2 \int_0^1 \xi^2 \csc\left(\frac{1}{2} \pi \xi\right) d\xi \right. \\
 \left. - \frac{1}{4} \pi^2 \int_1^{(2/\pi)\theta} \xi \csc\left(\frac{1}{2} \pi \xi\right) d\xi \right] (\sin \theta - \theta \cos \theta) \quad (44)
 \end{aligned}$$

where  $k_1 = -1.3253$ . For the Terrill–Thomas model, a similar expression is obtained, namely,

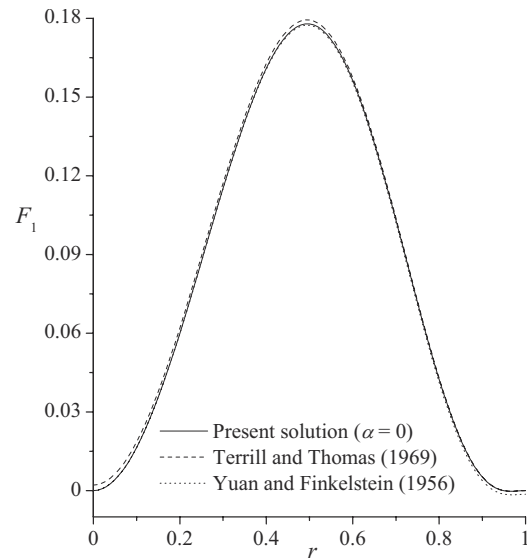


**Fig. 7** Comparison between the present solution and those obtained by Yuan and Finkelstein [33] and Terrill and Thomas [34]

$$\begin{aligned}
 F = \sin \theta + 2\varepsilon \left\{ \frac{1}{2} \pi \left[ 1 - 4 \pi^{-1} \beta_1 \right. \right. \\
 \left. \left. - \frac{1}{8} \pi^2 \int_1^{(2/\pi)\theta} \xi^2 \csc\left(\frac{1}{2} \pi \xi\right) d\xi \right] \cos \theta - \left( \frac{3}{2} - 4 \pi^{-1} \beta_1 \sin \theta \right) \right. \\
 \left. + \left( \frac{3}{2} - 4 \pi^{-1} \beta_1 - \frac{1}{8} \pi^2 \int_1^{(2/\pi)\theta} \xi \csc\left(\frac{1}{2} \pi \xi\right) d\xi \right) (\sin \theta \right. \\
 \left. - \theta \cos \theta) \right\} \quad (45)
 \end{aligned}$$

where  $\beta_1 = -k_1/\pi$ . Given that Fig. 7 is focused on  $F_1$  only, one may infer that these solutions, which share the same leading order part  $F_0$ , agree remarkably well irrespective of  $\varepsilon$ . This comparison concludes our presentation of the first order viscous mean flow analysis for this problem. It is hoped that the approximation furnished here could be used as a starting point in modeling internal burning hybrid cylinders.

#### 4 Conclusions

In this study, a rotational model is presented as a means to describe the basic gas dynamics in a full-length hybrid engine with circular bore. Our idealization is based on slightly viscous, rotational, and incompressible motion in conjunction with a harmonic injection profile at the chamber head end. The mean flow emerging from sidewall and endwall mass addition is rotational and satisfies the no slip condition at the wall. The solution may be helpful to point out, especially that its parameters,  $U_0$  and  $U_w$ , can be suitably adjusted to mimic the bulk gas motion reported in some hybrid geometry. It can also permit the investigation of hydrodynamic instability of the mean flow with head end injection. Finally, a formulation that incorporates viscosity is discussed and shown to compare favorably with the regularly perturbed solutions for the nondeformable porous cylinder obtained by Yuan and Finkelstein [33] and Terrill and Thomas [34]. Overall the effects of viscosity are found to be small except near the centerline. In hindsight, the models presented here constitute a first approximation to the bulk gaseous motion that arises in hybrid chambers exhibiting a circular port. In the past, only uniform (parallel) flows were used to describe the streamtube motion above the propellant

surface. The rotational, two-component, axisymmetric models can be used to represent the so-called outer field in a more comprehensive study that seeks to account for thermal effects. The advent of progressively more accurate outer flow approximations, such as the ones presented here, can thus be essential in the treatment of thermal boundary layers forming above the propellant surface.

## Acknowledgment

This project was sponsored by the National Science Foundation through Grant No. CMMI-0928762.

## Nomenclature

- $a$  = chamber radius  
 $p$  = normalized pressure,  $\bar{p}/(\rho U_w^2)$   
 $Re$  = wall injection Reynolds number,  $U_w a / \nu$   
 $r$  = normalized radial coordinate,  $\bar{r}/a$   
 $\mathbf{u}$  = normalized velocity  $(\bar{u}_r, \bar{u}_z)/U_w$   
 $U_0$  = head end injection velocity,  $\bar{u}_z(0, 0)$   
 $u_0$  = normalized injection velocity,  $U_0/U_w$   
 $u_h$  = head end injection parameter,  $U_0/(\pi U_w)$   
 $U_w$  = wall injection velocity,  $-\bar{u}_r(a, \bar{z})$   
 $z$  = normalized axial coordinate,  $\bar{z}/a$   
 $\varepsilon$  = viscous parameter,  $1/Re = \nu/(U_w a)$   
 $\nu$  = kinematic viscosity,  $\mu/\rho$   
 $\rho$  = density  
 $\Omega$  = vorticity,  $\nabla \times \mathbf{u}$

## Subscripts and Symbols

- $h$  = property at the head end  
 $r$  = radial component or partial derivative  
 $w$  = property at the sidewall  
 $z$  = axial component or partial derivative  
 $-$  = overbars denote dimensional variables

## References

- Chiaverini, M. J., Serin, N., Johnson, D. K., Lu, Y.-C., Kuo, K. K., and Risha, G. A., 2000, "Regression Rate Behavior of Hybrid Rocket Solid Fuels," *J. Propul. Power*, **16**(1), pp. 125–132.
- Chiaverini, M. J., Kuo, K. K., Peretz, A., and Harting, G. C., 2001, "Regression-Rate and Heat-Transfer Correlations for Hybrid Rocket Combustion," *J. Propul. Power*, **17**(1), pp. 99–110.
- Jenkins, R. M., and Cook, J. R., 1995, "A Preliminary Analysis of Low Frequency Pressure Oscillations in Hybrid Rocket Motors," 31st AIAA/ASME/SAE/ASEE Joint Propulsion Conference, San Diego, CA, Paper No. 95-2690.
- Krier, H., and Kerzner, H., 1972, "An Analysis of the Chemically Reacting Boundary Layer During Hybrid Combustion," AIAA/SAE Eighth Joint Propulsion Specialist Conference, New Orleans, LA, Paper No. 72-1144.
- Knuth, W. H., Chiaverini, M. J., Sauer, J. A., and Gramer, D. J., 2002, "Solid-Fuel Regression Rate Behavior of Vortex Hybrid Rocket Engines," *J. Propul. Power*, **18**(3), pp. 600–609.
- Karabeyoglu, M. A., Altman, D., and Cantwell, B. J., 2002, "Combustion of Liquefying Hybrid Propellant: Part 1, General Theory," *J. Propul. Power*, **18**(3), pp. 610–620.
- Karabeyoglu, M. A., and Cantwell, B. J., 2002, "Combustion of Liquefying Hybrid Propellant: Part 2, Stability and Liquid Films," *J. Propul. Power*, **18**(3), pp. 621–630.
- Kuo, K., and Chiaverini, M. J., 2007, *Challenges of Hybrid Rocket Propulsion in the 21st Century, Fundamentals of Hybrid Rocket Combustion and Propulsion*, K. Kuo and M. J. Chiaverini, eds., AIAA Progress in Astronautics and Aeronautics, Washington, DC, pp. 591–636.
- Culick, F. E. C., 1966, "Rotational Axisymmetric Mean Flow and Damping of Acoustic Waves in a Solid Propellant Rocket," *AIAA J.*, **4**(8), pp. 1462–1464.
- Taylor, G. I., 1956, "Fluid Flow in Regions Bounded by Porous Surfaces," *Proc. R. Soc. London, Ser. A*, **234**(1199), pp. 456–475.
- Dauenhauer, E. C., and Majdalani, J., 2003, "Exact Self-Similarity Solution of the Navier-Stokes Equations for a Porous Channel with Orthogonally Moving Walls," *Phys. Fluids*, **15**(6), pp. 1485–1495.
- Baum, J. D., Levine, J. N., and Lovine, R. L., 1988, "Pulsed Instabilities in Rocket Motors: A Comparison Between Predictions and Experiments," *J. Propul. Power*, **4**(4), pp. 308–316.
- Sabnis, J. S., Gibeling, H. J., and McDonald, H., 1989, "Navier-Stokes Analysis of Solid Propellant Rocket Motor Internal Flows," *J. Propul. Power*, **5**(6), pp. 657–664.
- Dunlap, R., Willoughby, P. G., and Hermsen, R. W., 1974, "Flowfield in the Combustion Chamber of a Solid Propellant Rocket Motor," *AIAA J.*, **12**(10), pp. 1440–1442.
- Dunlap, R., Blackner, A. M., Waugh, R. C., Brown, R. S., and Willoughby, P. G., 1990, "Internal Flow Field Studies in a Simulated Cylindrical Port Rocket Chamber," *J. Propul. Power*, **6**(6), pp. 690–704.
- Yamada, K., Goto, M., and Ishikawa, N., 1976, "Simulative Study of the Erosive Burning of Solid Rocket Motors," *AIAA J.*, **14**(9), pp. 1170–1176.
- Brown, R. S., Blackner, A. M., Willoughby, P. G., and Dunlap, R., 1986, "Coupling between Acoustic Velocity Oscillations and Solid Propellant Combustion," *J. Propul. Power*, **2**(5), pp. 428–437.
- Proudman, I., 1960, "An Example of Steady Laminar Flow at Large Reynolds Number," *J. Fluid Mech.*, **9**(04), pp. 593–602.
- Majdalani, J., Vyas, A. B., and Flandro, G. A., 2002, "Higher Mean-Flow Approximation for a Solid Rocket Motor with Radially Regressing Walls," *AIAA J.*, **40**(9), pp. 1780–1788.
- Majdalani, J., Vyas, A. B., and Flandro, G. A., 2009, "Erratum on Higher Mean-Flow Approximation for a Solid Rocket Motor with Radially Regressing Walls," *AIAA J.*, **47**(1), pp. 286–286.
- Majdalani, J., Zhou, C., and Dawson, C. A., 2002, "Two-Dimensional Viscous Flow Between Slowly Expanding or Contracting Walls with Weak Permeability," *J. Biomech.*, **35**(10), pp. 1399–1403.
- Majdalani, J., and Zhou, C., 2003, "Moderate-to-Large Injection and Suction Driven Channel Flows with Expanding or Contracting Walls," *J. Appl. Math. Mech.*, **83**(3), pp. 181–196.
- Zhou, C., and Majdalani, J., 2002, "Improved Mean Flow Solution for Slab Rocket Motors with Regressing Walls," *J. Propul. Power*, **18**(3), pp. 703–711.
- Flandro, G. A., and Majdalani, J., 2003, "Aeroacoustic Instability in Rockets," *AIAA J.*, **41**(3), pp. 485–497.
- Majdalani, J., Flandro, G. A., and Roh, T. S., 2000, "Convergence of Two Flowfield Models Predicting a Destabilizing Agent in Rocket Combustion," *J. Propul. Power*, **16**(3), pp. 492–497.
- Majdalani, J., 2001, "Vorticity Dynamics in Isobarically Closed Porous Channels. Part I: Standard Perturbations," *J. Propul. Power*, **17**(2), pp. 355–362.
- Ugurtas, B., Avalon, G., Lupoglazoff, N., Vuillot, F., and Casalis, G., 2000, *Stability and Acoustic Resonance of Internal Flows Generated by Side Injection, Solid Propellant Chemistry, Combustion, and Motor Interior Ballistics*, Vol. 185, V. Yang, T. B. Brill, and W.-Z. Ren, eds., AIAA Progress in Astronautics and Aeronautics, Washington, DC, pp. 823–836.
- Majdalani, J., and Saad, T., 2007, "The Taylor-Culick Profile with Arbitrary Headwall Injection," *Phys. Fluids*, **19**(9), pp. 093601.
- Muzzy, R., 1972, "Applied Hybrid Combustion Theory," AIAA/SAE Eighth Joint Propulsion Specialist Conference, New Orleans, LA, Paper No. 72-1143.
- Muzzy, R., and Wooldridge, C., 1967, "Internal Ballistic Considerations in Hybrid Rocket Design," *J. Spacecr. Rockets*, **4**(2), pp. 255–262.
- Marxman, G., Wooldridge, C., and Muzzy, R., 1964, "Fundamentals of Hybrid Boundary Layer Combustion," *Prog. Astronaut. Aeronaut.*, **15**, pp. 485–522.
- Kurdyumov, V. N., 2006, "Steady Flows in the Slender, Noncircular, Combustion Chambers of Solid Propellants Rockets," *AIAA J.*, **44**(12), pp. 2979–2986.
- Yuan, S. W., and Finkelstein, A. B., 1956, "Laminar Pipe Flow with Injection and Suction through a Porous Wall," *ASME Trans. J. Appl. Mech.*, **78**(3), pp. 719–724.
- Terrill, R. M., and Thomas, P. W., 1969, "On Laminar Flow Through a Uniformly Porous Pipe," *Appl. Sci. Res.*, **21**(1), pp. 37–67.